Available online at www.sciencedirect.com
SCIENCE DIRECT®
Journal of Sound and Vibration 286 (2005) 507–527
JOURNAL OF SOUND AND VIBRATION
www.elsevier.com/locate/jsvi

Real-time measurement of wave components and intensity in a beam in the presence of a near field

B.R. Mace[a,*], C.R. Halkyard[b], H.M. El-Khatib[a]

[a]*Institute of Sound and Vibration Research, University of Southampton, Highfield, Southampton SO17 1BJ, UK*
[b]*Department of Mechanical Engineering, The University of Auckland, Private Bag 92019, Auckland, New Zealand*

Received 14 February 2003; received in revised form 11 October 2004; accepted 12 October 2004
Available online 5 January 2005

Abstract

A method is described by which the individual flexural wave components in a beam can be measured in real time. Attention is focussed on the case in which two propagating waves and a single near-field wave exist, although the case of two near fields is also considered. Because the presence of the near field is included, the measurements can be taken close to the force, boundary or discontinuity from which the near field arises. Potential applications include intensity measurement, active control and adaptive-passive vibration control.

The wave components are measured by digitally filtering and combining the outputs of an array of sensors, with an array of three, equally spaced sensors being considered in detail. The filters are designed in the frequency domain using a wave decomposition approach, and implemented in the time domain as FIR filters. Design, implementation and performance issues are discussed and an experimental implementation described. It is seen that accurate estimates of the amplitudes of the wave components can be obtained using FIR filters of moderate order, and that the method is relatively insensitive to sensor miscalibration and measurement noise.

*Corresponding author. Tel.: +44 23 8059 2344; fax: +44 23 8059 3190.
E-mail address: brm@isvr.soton.ac.uk (B.R. Mace).

0022-460X/$ - see front matter © 2004 Elsevier Ltd. All rights reserved.
doi:10.1016/j.jsv.2004.10.017

Nomenclature

a	sensor location
EI	bending stiffness
f	frequency (Hz)
f_s	sampling frequency
g	filter impulse response, FIR filter coefficient
G	filter frequency response
H	$i\omega G$
k	wavenumber
m	time step
n_d	filter delay
n_t	number of terms in FIR filter
p	arbitrary variable, distributed load
$\mathbf{S}$	sensor matrix
t	time
v	velocity
w	beam displacement
x	position along beam
$\mathbf{Y}$	vector of sensor outputs
θ	beam rotation
ε	calibration error
λ	wavelength
ρ	mass per unit length
σ	filter weight function
ϕ	wave amplitude
ω	frequency

Subscripts

j	sensor number
k	filter coefficient number
m	time step number
n	value at Nyquist frequency
N	near field

1. Introduction

Knowledge of the amplitudes of the various wave components that can propagate in a structure can provide valuable information concerning the vibrations of a structure, especially at higher frequencies. Typically, these wave amplitudes are estimated retrospectively in the frequency domain, by processing blocks of time-domain data. While this approach is satisfactory in many situations, applications exist for which real-time estimates are more useful. These include the measurement of vibrational energy flow [1,2], particularly that due to transient and other non-stationary excitation, active vibration control [3–5], where real-time estimates of the amplitude of a given wave component can be used as a reference or error signal, and adaptive-passive control, where the contribution of a given wave component can again be used to quantify the performance of the system and adapt its properties. The specific case of active control in the presence of a near field is considered in detail in a companion paper [6].

This paper describes the real-time measurement of the amplitude of individual wave components in a beam undergoing flexural vibration. The case considered is that in which two propagating waves and a single near-field wave exist. The amplitude of the wave component (e.g. the positive-going propagating wave component) at any particular time will, in general, be a sum of a number of different frequency components. The real-time measurements are provided by filtering the outputs of an array of sensors, with the specific case of three, equally spaced sensors being considered in detail. The approach is similar to that described in Ref. [2], where far-field conditions were assumed. However, those conditions mean that the sensor array must be located at a significant distance from any discontinuity, excitation point or boundary, since these features create a near field which affects the sensor outputs if they are placed within about half a wavelength of the near-field source. This precludes the use of the far-field method in many

practical situations, or severely restricts the frequency range over which accurate measurements can be taken. The case considered here allows for the existence of the near field produced by an 'upstream' source, so that accurate measurements can be taken so long as any near field produced by a 'downstream' source is negligible.

The technique used is based on wave decomposition and reconstruction, and follows the approach of Ref. [2] except that here a near-field wave is also taken into account. The outputs of the sensors are digitally filtered. The filters are designed using a wave decomposition approach in the frequency domain and implemented in the time domain as FIR filters. In the next section, some results concerning wave motion in beams are reviewed. The required filter frequency responses are then determined, and issues concerning the filter design, implementation and performance are discussed. Application to real-time intensity measurement is considered. Finally some experimental results are presented. The general case in which there are two near fields is amenable to the same approach and is discussed in Appendix A.

2. Measurement of bending wave amplitudes

Consider a thin beam lying along the x-axis. If the effects of shear deformation and rotary inertia can be neglected, then the displacement $w(x,t)$ satisfies

$$\mathrm{EI}\,\frac{\partial^4 w}{\partial x^4}+\rho\frac{\partial^2 w}{\partial t^2}=p(x,t), \tag{1}$$

where EI and ρ are the bending stiffness and mass per unit length of the beam and $p(x,t)$ is the applied force per unit length. A list of symbols is given in the nomenclature.[1]

Suppose now that all quantities vary time harmonically as $\exp(\mathrm{i}\omega t)$. The beam displacement can be written as

$$w(x,t)=\mathrm{Re}\{W(x,\omega)\mathrm{e}^{\mathrm{i}\omega t}\}. \tag{2}$$

In this paper, the notation is adopted in which the lower- and upper-case symbols (e.g. $w(t)$ and $W(\omega)$) represent the same variable in the time and frequency domains, respectively, and the explicit time dependence will normally be suppressed. In a region in which no applied forces act, the displacement can be expressed as the sum of wave components

$$W(\omega)=\Phi_W^+(\omega)\mathrm{e}^{-\mathrm{i}kx}+\Phi_{N,W}^+(\omega)\mathrm{e}^{-kx}+\Phi_W^-(\omega)\mathrm{e}^{\mathrm{i}kx}+\Phi_{N,W}^-(\omega)\mathrm{e}^{kx}, \tag{3}$$

where $\Phi_W^{\pm}(\omega)$ are the complex amplitudes of the positive- and negative-going propagating waves at frequency ω and $\Phi_{N,W}^{\pm}(\omega)$ those of the positive- and negative-going near fields. The near-field components decay exponentially in the positive and negative x-directions, respectively, and are thus spatially localised, decaying in amplitude by a factor of about 0.04 in half a wavelength. In Eq. (3), $k=\sqrt[4]{\rho\omega^2/\mathrm{EI}}$ is the wavenumber. In the presence of damping, k has a (usually small) negative imaginary part so that the amplitude of a propagating wave component decays gradually in the direction of propagation. In this paper, it will be assumed that this decay is negligible over distances of the order of the sensor separations.

[1]The lower case symbol (e.g. $p(t)$) is used to represent a variable in the time domain, while the upper case, $P(\omega)$, represents the same variable in the frequency domain.

The subscript W in Eq. (3) indicates that it is the transverse displacement $W(\omega)$ of the beam that has been decomposed into the wave components Φ_W. The wave amplitudes Φ_W are thus referred to as displacement wave amplitudes. However, all response quantities (transverse velocity, acceleration, shear force, etc.) vary time harmonically under the passage of a wave. Thus one could equally define the amplitudes of the wave components in terms of the amplitude of any such response quantity. For example one may equally refer to velocity waves, which have amplitudes $\Phi_V = \mathrm{i}\omega\Phi_W$, or acceleration waves which have amplitudes $\Phi_A = -\omega^2\Phi_W$: the superposition of such waves then gives the velocity or acceleration of the waveguide, respectively. Whichever is chosen is purely a matter of convenience and might depend, e.g. on the particular output signal from the sensors.

2.1. Frequency domain decomposition

The aim is to measure the instantaneous amplitudes of the individual wave components in real time using various sensors. Generally, these will be the sum of contributions at various frequencies. In this paper, the particular case of the array of sensors shown in Fig. 1 is considered. The array comprises three equally spaced sensors located at $x = 0, \pm a$. The sensors are assumed to give point measurements of the same kind, for example acceleration or velocity, e.g. but the method can easily be extended to an array containing sensors of different kinds or distributed sensors (e.g. strain gauges of non-negligible length).

The outputs of the sensors are filtered and combined to yield estimates of the amplitudes of the different wave components at the centre of the array, $x = 0$. These filters are referred to as wave filters or wave component filters. The filters are designed in the frequency domain as described in this section. They are subsequently implemented in the time domain by convolving the sensor outputs with the impulse responses of various filters. The implemented filters have frequency responses which approximate the idealised designs.

In the design of the wave filters, it is assumed that the near-field Φ_N^- is negligible, although its contaminating effects are included in the simulations described later. This implies that any discontinuities, forces, boundaries, etc. are assumed to be far enough to the right (half a wavelength or so) so that the consequent near field has decayed to a negligible level. The positive-going near-field Φ_N^+ may have a significant amplitude, however, so that measurements can be taken arbitrarily close to such a source. It is, however, straightforward to include the near-field Φ_N^- (see Appendix A).

Suppose the sensors measure displacement. If the near-field Φ_N^- is ignored, then, for the frequency component ω, the displacement in the region around the array can be written as

$$W(x,\omega) = \Phi^+ \mathrm{e}^{-\mathrm{i}kx} + \Phi_N^+ \mathrm{e}^{-kx} + \Phi^- \mathrm{e}^{\mathrm{i}kx}. \tag{4}$$

The subscript W is omitted for simplicity. The vector of sensor outputs is then

$$\mathbf{Y}(\omega) = \begin{Bmatrix} W(-a,\omega) \\ W(0,\omega) \\ W(a,\omega) \end{Bmatrix} \tag{5}$$

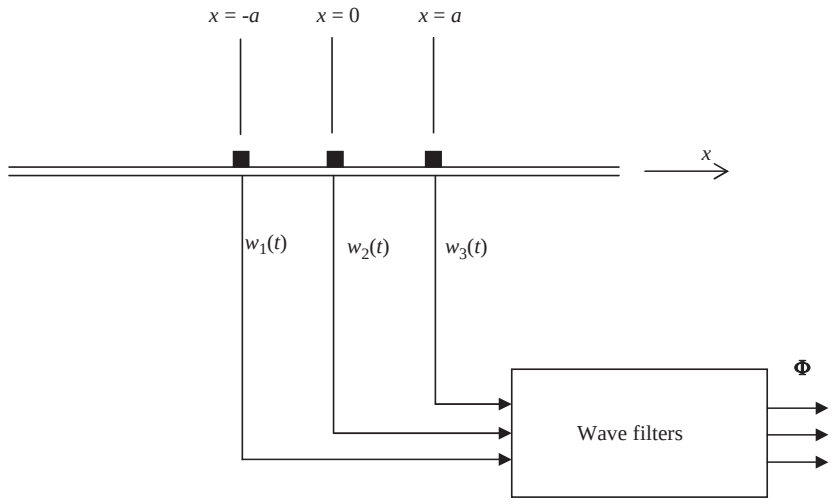

Fig. 1. Near-field sensor array comprising three sensors.

and hence

$$\mathbf{Y}(\omega) = \mathbf{S}(\omega)\mathbf{\Phi}(\omega), \quad \mathbf{\Phi}(\omega) = \begin{Bmatrix} \Phi^{+} \\ \Phi^{-} \\ \Phi_{N}^{+} \end{Bmatrix}, \tag{6}$$

where the sensor matrix

$$\mathbf{S}(\omega) = \begin{bmatrix} \mathrm{e}^{\mathrm{i}ka} & \mathrm{e}^{-\mathrm{i}ka} & \mathrm{e}^{ka} \\ 1 & 1 & 1 \\ \mathrm{e}^{-\mathrm{i}ka} & \mathrm{e}^{\mathrm{i}ka} & \mathrm{e}^{-ka} \end{bmatrix}. \tag{7}$$

The wave amplitudes are consequently given by

$$\mathbf{\Phi}(\omega) = \mathbf{G}(\omega)\mathbf{Y}(\omega), \quad \mathbf{G}(\omega) = \mathbf{S}^{-1}(\omega). \tag{8}$$

The frequency response matrix $\mathbf{G}(\omega)$ can be found by inverting $\mathbf{S}(\omega)$ but the resulting expression is not given here. The determinant of $\mathbf{S}$ equals $4\mathrm{i}\sin ka(\cosh ka - \cos ka)$, and hence $\mathbf{S}$ is singular if the separation a is half a wavelength: this imposes an (quite high) upper frequency limit for the array.

As defined above, the matrix $\mathbf{G}$ provides wave amplitudes of the same response variable as the sensor outputs, i.e. displacement measurements give displacement wave amplitudes. Similarly, acceleration measurements would give acceleration wave amplitudes. This need not be the case, however. For example if the sensors measure velocity, then $\mathbf{G}$ would provide estimates of velocity-wave amplitudes, while $\mathrm{i}\omega\mathbf{G}$ and $\mathbf{G}/(\mathrm{i}\omega)$ would provide estimates of acceleration-wave and displacement-wave amplitudes, respectively.

2.2. Time-domain reconstruction

In general, more than one frequency component will be present and each wave component will be the superposition of these various frequency components. Thus

$$\phi(t) = F^{-1}\{\mathbf{\Phi}(\omega)\} = \int_{-\infty}^{\infty} \mathbf{\Phi}(\omega) \mathrm{e}^{\mathrm{i}\omega t}\, \mathrm{d}\omega, \tag{9}$$

where $F^{-1}\{\cdot\}$ is the inverse Fourier transform. Since the inverse transform of a product is equal to the convolution of the individual inverse transforms, then

$$\phi(t) = \mathbf{g}(t) * \mathbf{y}(t), \tag{10}$$

where * denotes convolution and $\mathbf{g}(t)$ is a matrix of impulse responses, which are the inverse Fourier transforms of the elements of $\mathbf{G}(\omega)$. In a practical implementation an approximation to these is found. The examples below involve a digital implementation, with FIR filters being used.

The steps in implementing the wave filters are thus to specify the details of the sensor array, to determine the matrices $\mathbf{S}(\omega)$ and $\mathbf{G}(\omega)$, and to design filters whose impulse responses approximate $\mathbf{g}(t)$ to acceptable accuracy.

One issue that arises is that the required filters are typically non-causal, so that $g(t)$ is non-zero for $t<0$. This is not surprising, since estimates at any particular time are made for the amplitudes of the wave components at $x = 0$ from sensor measurements taken at various locations. It takes some time for waves to propagate from one location to another, so exact estimation of the amplitudes of the wave components requires knowledge of the future output of the downstream sensor. In practice, these effects are not important for applications where 'real-time' performance is not crucial, such as response and intensity estimation—in effect, a small delay can be incorporated into the filtering process before the measurement is produced. These time delays have more profound consequences for applications such as active control.

3. FIR filter implementation

Practical implementations will be predominantly digital, with FIR filters being used in this paper. The sensor outputs are sampled at the sampling frequency f_s, with the Nyquist frequency (and cut-off frequency of the anti-aliasing filters) defining a maximum frequency of interest and hence a maximum sensor spacing. The estimated amplitude of a wave component at time step m is then

$$\phi_m = \sum_{j=1,3} \left(\sum_{k=0,K} g_{j,k} y_{j,m-k} \right), \tag{11}$$

where the length of the filters is $K+1$. The implemented filters are causal and of finite length. They are consequently approximations to the ideals defined above.

There are a number of ways of designing FIR filters. Here the 'time delay' approach described in Ref. [2] is adopted. A $n_t = (2n_d + 1)$ term filter is designed by time-delaying the filters in $\mathbf{G}$ by n_d time steps, which is equivalent to multiplying $\mathbf{G}$ by $\exp(-\mathrm{i}\omega n_d/f_s)$. A weighted least-squares procedure is then used to fit the implemented frequency response $\mathbf{G}$ to that of the appropriate

element of $\mathbf{G}$, i.e. so as to minimise the sum over frequency of $(\sigma(\omega)|G(\omega) - \hat{G}(\omega)|^2)$, where $\sigma(\omega)$ is a chosen weight function. The causal filter will then produce an estimate of ϕ_m at time step $m+n_d$. Only small values of n_d are required.

The accuracy of the implemented filters depends on the number of terms and is generally worst for low frequencies and for frequencies close to the Nyquist frequency. Consequently, these frequency ranges can be zero-weighted in the least-squares estimation if required. In practice, however, the low- and high-frequency components of the signals will often be filtered out (e.g. by the anti-aliasing filters and by a.c. coupling) and this will substantially ameliorate the effects of the poor approximation in these frequency ranges.

Another issue concerns exactly which frequency responses to implement. Here two types are considered, these being $\mathbf{G}$ and $\mathbf{H} = \mathrm{i}\omega\mathbf{G}$. The first is a direct implementation of the frequency domain design. The second, with an additional term $(\mathrm{i}\omega)$, in effect estimates velocity wave amplitudes from sensor measurements of displacement, rather than displacement wave amplitudes. The numerical examples show a somewhat better approximation for a given number of terms (primarily because the filters in $\mathbf{G}$ become infinite at zero frequency while those in $\mathbf{H}$ vary much less with frequency) and a somewhat better performance.

3.1. Numerical examples

In this section some numerical examples are presented. The filters were designed using the Matlab function *invfreqz*, with the ideal frequency responses defined at 256 equally spaced frequencies up to the Nyquist frequency f_n. The implemented FIR filter coefficients were found using uniform weighting over the frequency range from $0.1f_n$ to $0.9f_n$ and zero weighting elsewhere. The results are given for a sensor spacing $a = 0.1\,\lambda_n$, where λ_n is the bending wavelength at the Nyquist frequency.

Figs. 2–5 show various ideal and implemented filter frequency responses for wave amplitude filters of the two types described above with $n_d = 5$. Figs. 2 and 4 show the filters for the downstream propagating wave $\phi^+(t)$ (e.g. G_{11}, G_{12}, G_{13}) while Figs. 3 and 5 show the filters for the near-field wave $\phi_N^+(t)$ (e.g. G_{31}, G_{32}). Note that $G_{2j} = G_{1j}^*$, while the near-field filters G_{3j} are real with $G_{33} = G_{31}$. Generally, the real part of G is approximated better than the imaginary part, while the approximation for H tends to be better than that for G. This is due in part to the fact that the filter coefficients are constrained to be real, and hence the imaginary part of $\hat{G}$ must be zero at both zero and the Nyquist frequency, and in part to the fact that G becomes infinite at zero frequency. Increasing the filter length gives better approximation. Figs. 6 and 7 show cases with $n_d = 15$, while Fig. 8 shows $\hat{G}_{11}$ for various n_d. A good approximation is produced by filters of relatively low order.

3.2. Performance considerations

In practice, the performance of the system is compromised by a number of factors so that the measured wave amplitudes $\widehat{\mathbf{\Phi}}$ will differ from the actual wave amplitudes $\mathbf{\Phi}$ for various reasons. First, the measured sensor outputs

$$\hat{\mathbf{Y}} = \mathrm{diag}(1 + \varepsilon_c)(\mathbf{Y} + \mathbf{S}_N^- \mathbf{\Phi}_N^-) + \mathbf{n}_y \tag{12}$$

differ from $\mathbf{Y}$. Here diag$(\cdot)$ is a diagonal matrix, ε_c represents sensor magnitude and phase miscalibration and $\mathbf{n}_y$ represents measurement noise. The term $\mathbf{S}_N^-$ gives the contribution due to the negative-going near field which is neglected in the design but which may, in practice, exist and will then contaminate the sensor outputs. Secondly, the implemented frequency responses $\widehat{\mathbf{G}}$ are only approximations to the ideals because of filter approximations. Finally, errors and uncertainties in the values of the parameters in the sensor array $\mathbf{S}$ (e.g. the wavenumber and the locations of the sensors in the examples above) mean that the actual matrix $\widehat{\mathbf{S}}$ differs from the matrix $\mathbf{S}$ of Eq. (7) from which the filters are designed.

The measured wave amplitudes are then

$$\widehat{\mathbf{\Phi}} = \widehat{\mathbf{G}}\widehat{\mathbf{Y}}, \tag{13}$$

where $\hat{\mathbf{Y}}$ is given by Eq. (12) and where $\mathbf{Y} = \widehat{\mathbf{S}}\mathbf{\Phi}$. Given that there are three sensors in the array, many factors affect the performance and clearly the situation can become very complicated.

3.2.1. Accuracy and cross-sensitivity

Suppose that $\hat{\mathbf{Y}} = \mathbf{Y}$ and that the sensor matrix $\mathbf{S}$ is known exactly, so that the measured amplitudes are

$$\widehat{\mathbf{\Phi}} = \widehat{\mathbf{G}}\mathbf{S}\mathbf{\Phi}. \tag{14}$$

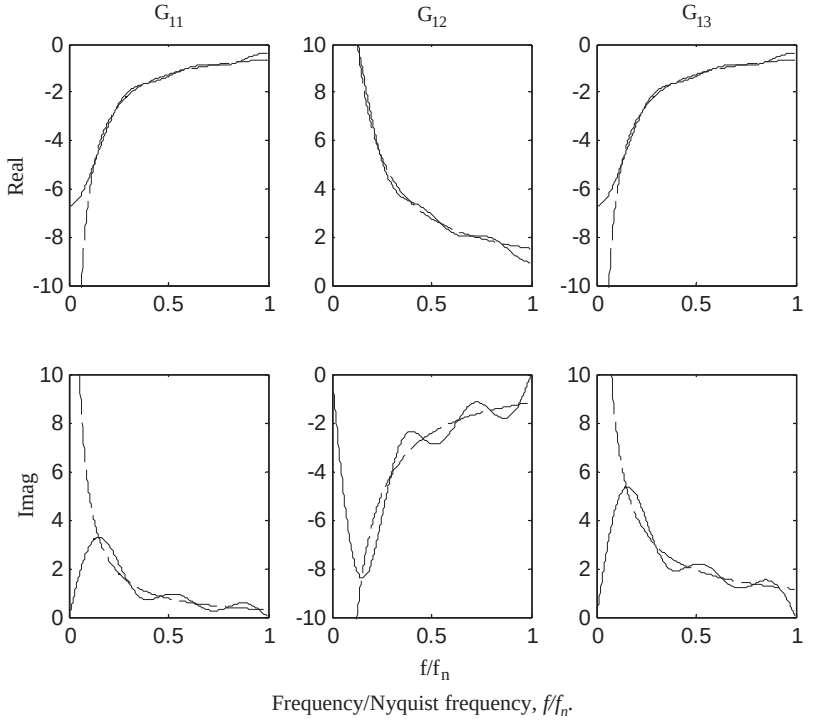

Fig. 2. Ideal (- - -) and implemented (—) downstream propagating wave amplitude filters G_{11}, G_{12} and G_{13}: $a = 0.1\,\lambda_n$, $n_d = 5$.

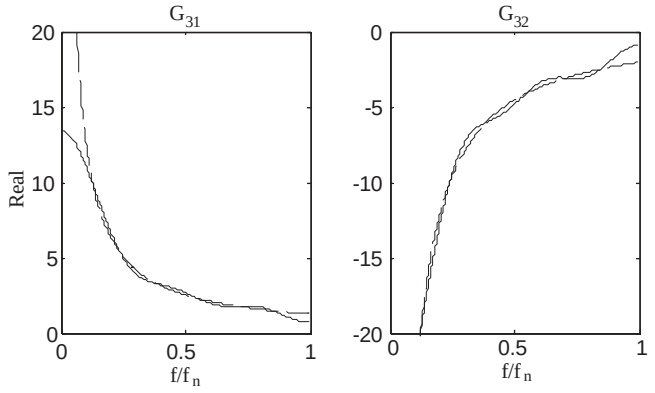

Fig. 3. Ideal (- - -) and implemented (—) near-field wave amplitude filters G_{31} and G_{32}: $a = 0.1\,\lambda_n$, $n_d = 5$.

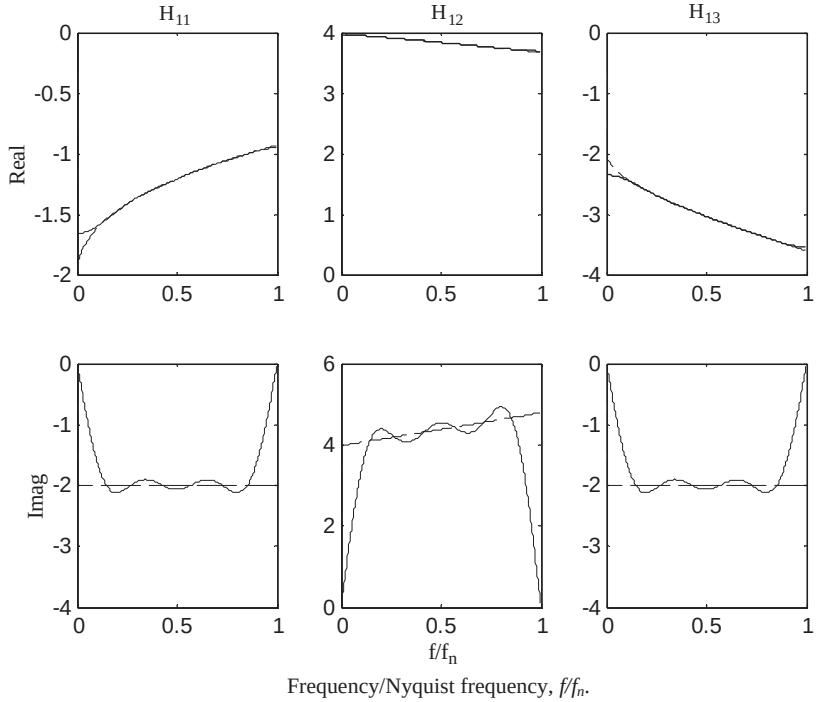

Fig. 4. Ideal (- - -) and implemented (—) downstream propagating wave amplitude filters H_{11}, H_{12} and H_{13}: $a = 0.1\,\lambda_n$, $n_d = 5$.

The accuracy (e.g. $|\widehat{\phi}^{+}/\phi^{+}|$, $|\hat{\phi}_N, \phi_N|$, etc.) and cross-sensitivity (e.g. $|\hat{\phi}^{+}/\phi^{-}|$, $|\hat{\phi}^{+}, \phi_N|$, etc.) of the measurements then depends only on inaccuracies in the filter matrix **G**. Fig. 9 shows examples for filters designed using $n_d = 5$ and 15. Generally, the measurements are accurate and fairly insensitive to the presence of other wave components except at low and high frequencies, and error decrease with increasing filter order, as one would expect.

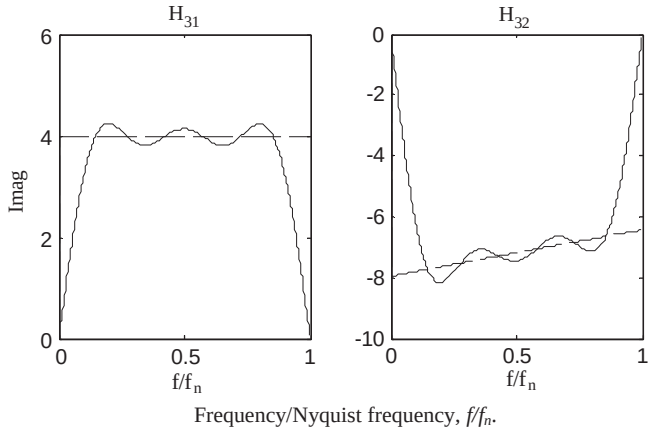

Fig. 5. Ideal (- - -) and implemented (—) near-field wave amplitude filters H_{31} and H_{32}: $a = 0.1\lambda_n$, $n_d = 5$.

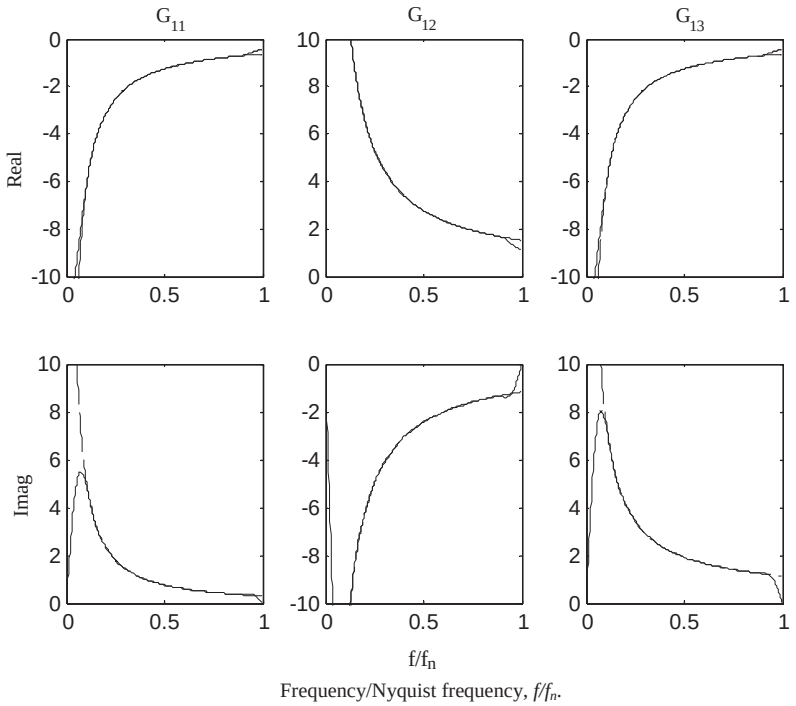

Fig. 6. Ideal (- - -) and implemented (—) downstream propagating wave amplitude filters G_{11}, G_{12} and G_{13}: $a = 0.1\,\lambda_n$, $n_d = 15$.

3.2.2. Sensor matrix uncertainty: sensitivity to wavenumber

Suppose now that the sensor outputs are perfect so that $\hat{\mathbf{Y}} = \mathbf{Y}$, while the implemented filters are perfect and hence $\mathbf{G}$ is known exactly. Errors now arise solely from inaccuracies in the sensor

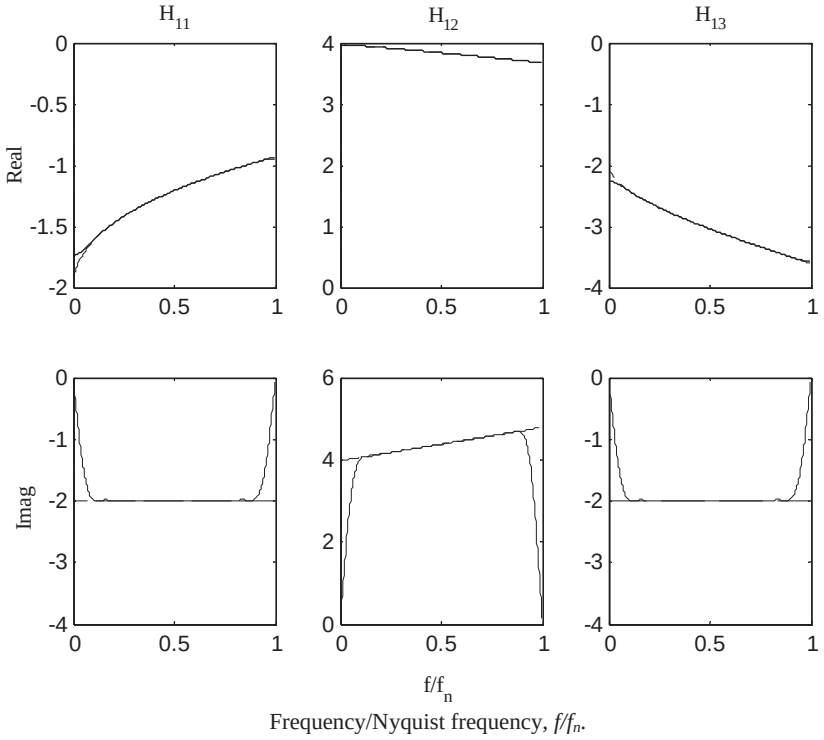

Fig. 7. Ideal (- - -) and implemented (—) downstream propagating wave amplitude filters H_{11}, H_{12} and H_{13}: $a = 0.1\,\lambda_n$, $n_d = 15$.

locations and the wavenumber in the sensor matrix $\hat{\mathbf{S}}$. The measured wave amplitudes are now $\hat{\mathbf{\Phi}} = \mathbf{G}\hat{\mathbf{S}}\mathbf{\Phi}$.

The sensitivity to a parameter μ (e.g. wavenumber, sensor location, etc.) is such that

$$\frac{\partial \mathbf{\Phi}}{\partial \mu} = \mathbf{G}\frac{\partial \mathbf{S}}{\partial \mu}\mathbf{\Phi}. \tag{15}$$

Errors in the estimated value of the wavenumber k produce errors in the measured wave amplitudes. As an example, Fig. 10 shows the relative errors in the measured wave amplitudes $|\delta\phi/\phi|$ caused by relative errors $\delta k/k$ in the wavenumber k. Clearly, the sensitivity to this error is fairly low, being approximately 1 or less.

3.2.3. *Sensor matrix uncertainty: sensitivity to sensor location*

It was assumed that the sensors are equally spaced, so that an error in sensor placement will produce errors in the measured wave amplitudes. For example, suppose that the rightmost sensor is attached at $x = x_1$ instead of $x = a$. The sensitivity to this misplacement is then found from

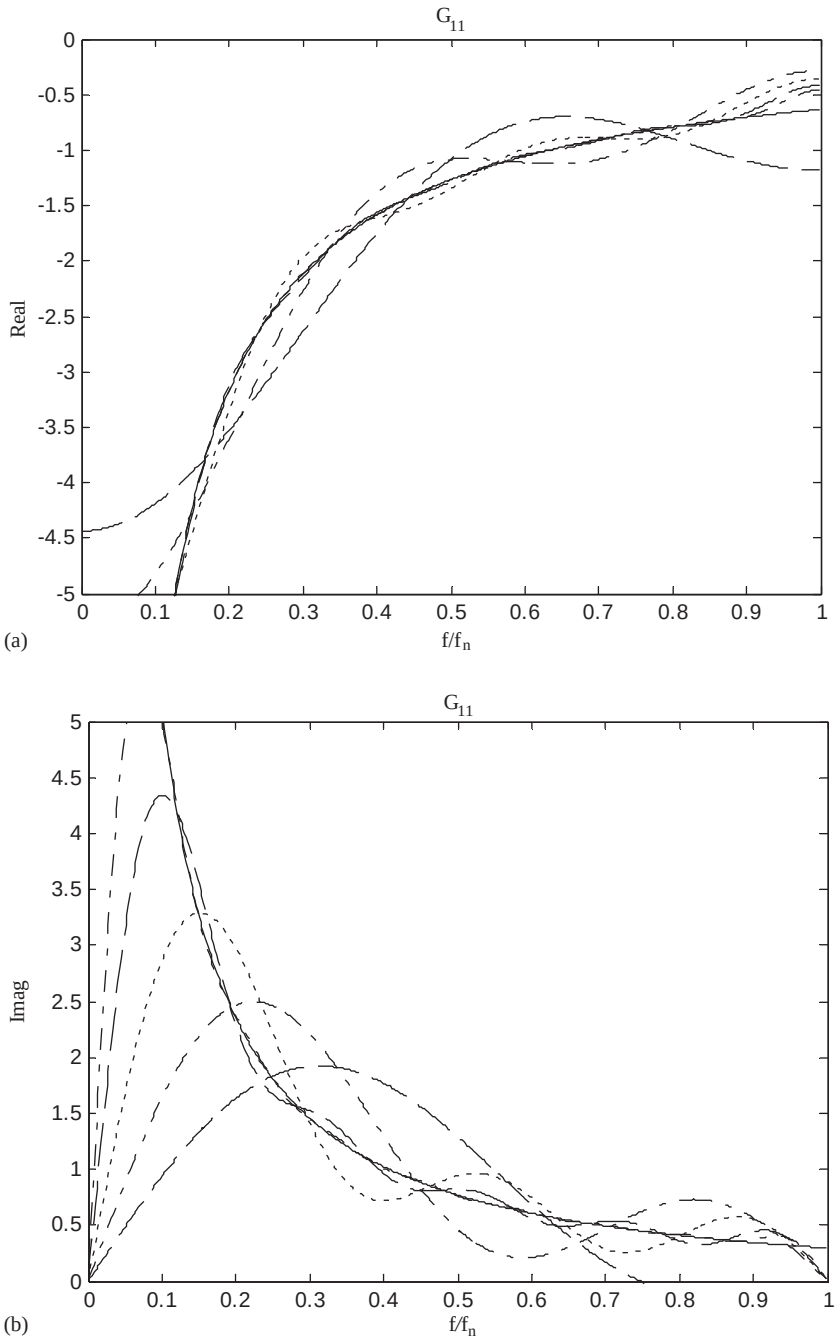

Fig. 8. Ideal and implemented downstream propagating wave amplitude filters G_{11}, $a = 0.1\lambda_n$, various n_d, (a) Re$\{G_{11}\}$ and (b) Im$\{G_{11}\}$: — ideal; – – – $n_d = 2$; - · - · - · $n_d = 3$; . . . . . $n_d = 5$; – – $n_d = 9$; - · - · - $n_d = 15$.

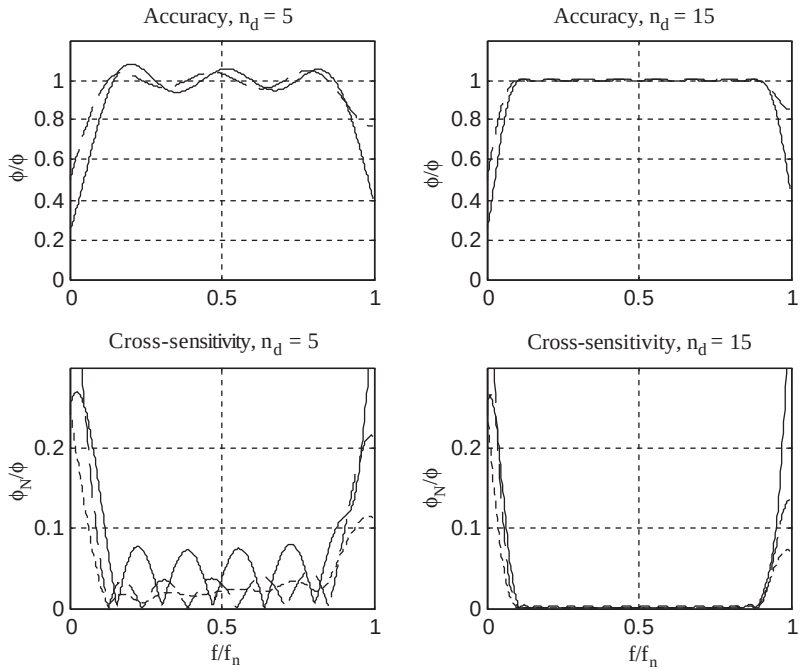

Fig. 9. Performance of three-sensor array, $a = 0.1\lambda_n$; $n_d = 5$ and 15: accuracy: $|\hat{\Phi}^+/\Phi^+|$; -----$|\hat{\Phi}_N^+/\Phi_N^+|$; cross-sensitivity: $|\hat{\Phi}^+/\Phi^-|$; ----- $|\hat{\Phi}_N^+/\Phi^\pm|$; .... $|\hat{\Phi}^+/\Phi_N^+|$.

Eq. (15) with

$$\frac{\partial \mathbf{S}}{\partial x_1} = k \begin{bmatrix} 0 & 0 & 0 \\ 0 & 0 & 0 \\ -\mathrm{i}\mathrm{e}^{-\mathrm{i}ka} & \mathrm{i}\mathrm{e}^{\mathrm{i}ka} & -\mathrm{e}^{-ka} \end{bmatrix}. \tag{16}$$

Fig. 11 shows the relative wave amplitude errors caused by relative placement errors $\delta x_1/a$. The sensitivity to this form of error can be large, especially at low frequencies where ka is small, and emphasises the need for accurate sensor placement. It also illustrates an advantage of the wave approach compared to the finite difference approach. The sensor spacing for the wave approach can be substantially larger than that for the finite difference approach, which requires that $ka \ll 1$. This larger sensor spacing can result in substantially reduced sensitivity to sensor misplacement. The sensitivity to any other sensor misplacements can be found by combining the results of this and the previous subsection.

3.2.4. Conditioning and the effects of noise and miscalibration

The condition number of the sensor matrix $\mathbf{S}$ is an indicator of the total effects of miscalibration, noise, etc. on the estimates and the resulting sensitivity of the matrix $\mathbf{G}$ to these sources of error. Fig. 12 shows this condition number for the example sensor array as a function

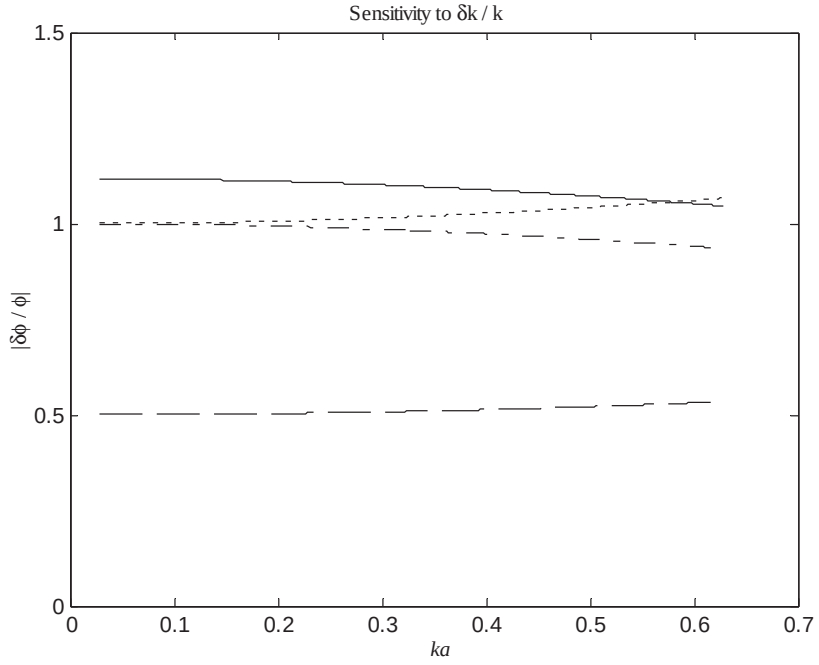

Fig. 10. Sensitivity of three-sensor array to $\delta k/k$: — $|\delta\Phi^+/\Phi^+|$; _ _ _ $|\delta\Phi^+/\Phi^-|$; - · - · $\left|\delta\Phi_N^+/\Phi^+\right|$; . . . .$|\delta\Phi_N^+/\Phi_N^+|$.

of frequency. At low frequencies the condition number is high, the sensors being closely spaced compared to the wavelength, but the condition number decreases with increasing frequency.

4. Measurement of intensity

As an illustrative application of the foregoing, consider the measurement of the instantaneous flow of energy along the beam, i.e. the structural intensity. This is given by

$$\mathrm{i}(x,t) = -q(t)v(t) - m(t)\dot{\theta}(t), \tag{17}$$

where

$$m(t) = \mathrm{EI}\,\frac{\partial^2 w}{\partial x^2}, \quad q(t) = -\mathrm{EI}\,\frac{\partial^3 w}{\partial x^3} \tag{18}$$

are the bending moment and shear force, respectively, while $v = \partial w/\partial t$ and $\dot{\theta} = \partial^2 w/\partial x\,\partial t$ are the translational and rotational velocities of the beam.

The same wave approach was developed in Ref. [2] for the far-field case where there are only propagating waves and only two sensors are required. Two methods were described. The first involves estimating the wave amplitudes and the energy flow associated with each. The second, and perhaps the simpler, is to estimate the bending moment and shear force directly, and hence to

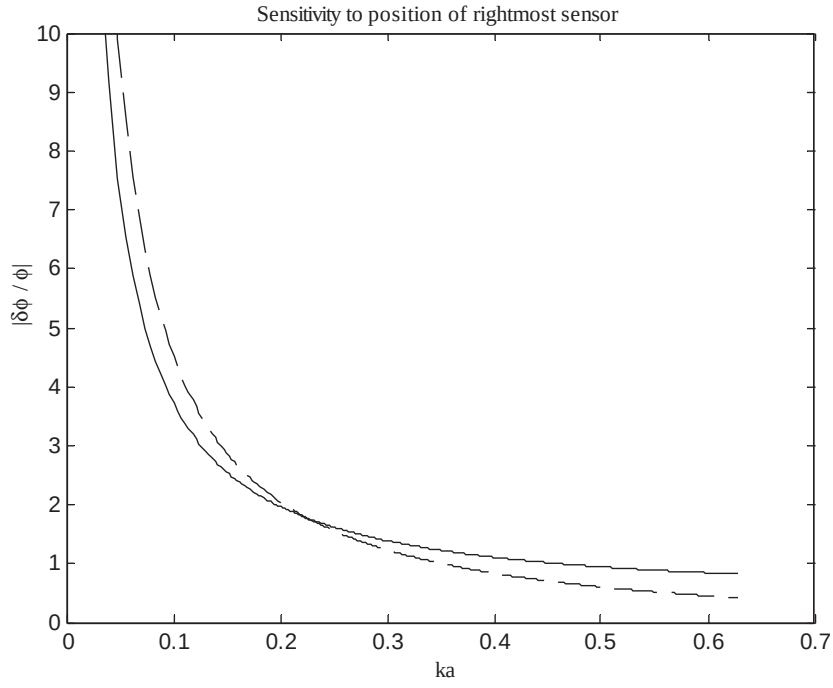

Fig. 11. Sensitivity of three-sensor array to placement of rightmost sensor, $\delta x_1/a$: — $|\delta\Phi^+/\Phi^+|$, $|\delta\Phi^-/\Phi^-|$; _ _ _ $|\delta\Phi_N^+/\Phi_N^+|$.

estimate the intensity from Eq. (17). This method will be outlined here when a near field is present. This approach is in contrast to the finite difference technique [1] which involves four sensors, equally and closely spaced. The wave approach is much more accurate and much less sensitive to miscalibration, errors in sensor spacing and so on, partly because only three sensors are required and partly because the sensors can be spaced further apart (up to one half-wavelength).

In the frequency domain the moment and shear are related to the wave amplitudes by

$$\begin{Bmatrix} M(\omega) \\ Q(\omega) \end{Bmatrix} = \mathrm{EI}\,k^2 \begin{bmatrix} -1 & -1 & 1 \\ -\mathrm{i}k & \mathrm{i}k & k \end{bmatrix} \begin{Bmatrix} \Phi_W^+(\omega) \\ \Phi_W^-(\omega) \\ \Phi_{N,W}^+(\omega) \end{Bmatrix} \tag{19}$$

and are hence related to the sensor measurements $\mathbf{Y}$ by

$$\begin{Bmatrix} M(\omega) \\ Q(\omega) \end{Bmatrix} = \left(\mathrm{EI}\,k^2 \begin{bmatrix} -1 & -1 & 1 \\ -\mathrm{i}k & \mathrm{i}k & k \end{bmatrix} \mathbf{S}^{-1}(\omega) \right) \mathbf{Y}(\omega). \tag{20}$$

Real-time estimates of the bending moment and the shear force can thus be found by time-domain reconstruction and FIR filter design as described in Sections 2.2 and 3, with the terms in the filter frequency responses being those in parentheses in Eq. (20), e.g. $\mathrm{EI}\,k^2 G_{11}$, $\mathrm{i}\,\mathrm{EI}\,k^3 G_{21}$, etc. These can be combined with real-time estimates of linear and angular velocity (either measured directly or

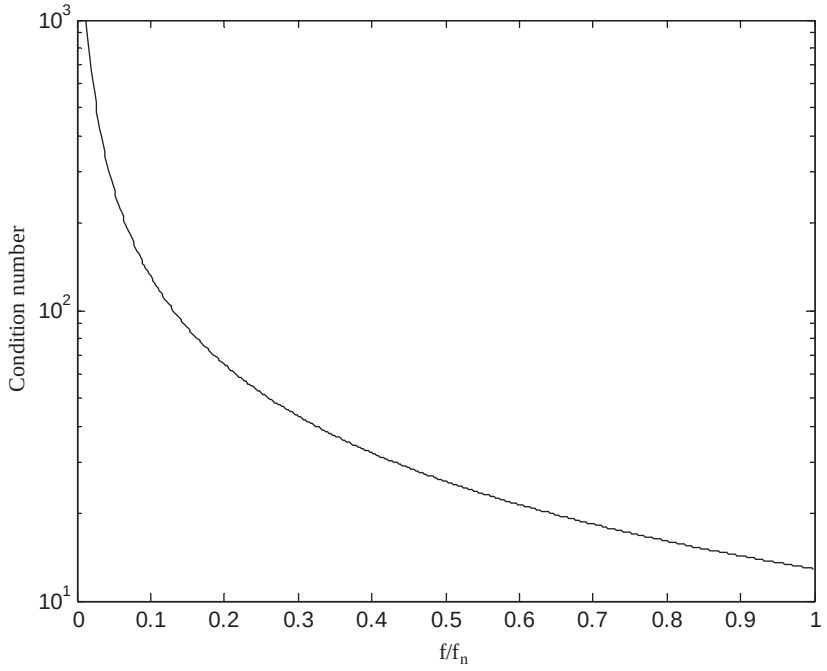

Fig. 12. Condition number of sensor matrix **S** for three-sensor array.

obtained via time-domain reconstruction) to yield a real-time estimate of instantaneous intensity using Eq. (18).

5. Experimental implementation

The experimental set-up comprised a steel beam of dimensions $50.6 \times 6.4 \times 5630$ mm suspended at four points along its length. One end was embedded in a sand box to reduce reflections. While wave component measurements can be taken equally in reverberant or non-reverberant conditions, the presence of the sandbox reduces any resonant effects, so that the spectra of the wave amplitudes incident on the sensors become more uniform. This ensures that relative and absolute measurement errors are more-or-less uniform over the whole frequency range. The beam was excited by a Ling V201 shaker and accelerations measured using PCB type 352C22 accelerometers. Test signals were generated and measurements processed in real time using a PC with Matlab, Simulink, the Real-Time Workshop and the Real-Time Windows Target. Other equipment included a power amplifier and reconstruction filters.

Various experiments were performed to illustrate the measurement of wave components. Throughout, the sampling rate was 1024 Hz. FIR filters were designed with zero weighting being applied apart from the frequency range from $0.1f_n$ to $0.9f_n$. The measured wavenumber of the beam was such that $k = 0.8269\sqrt{f}$.

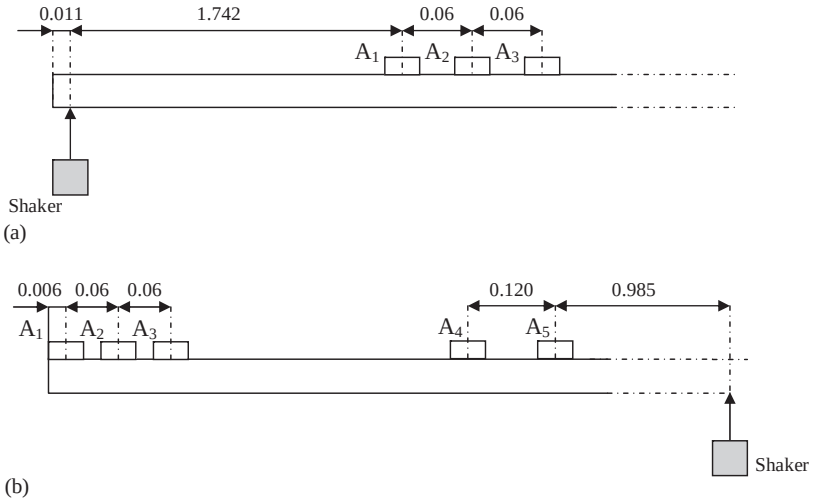

Fig. 13. Experimental configurations with locations of accelerometers and shaker indicated (all dimensions in m).

It is very difficult to make meaningful comparisons in the time domain, since no reference measurement of wave amplitude can be made. Furthermore, the time signals are contaminated by errors introduced by the poor approximation of the filters at low and high frequencies, so that visual comparison for broad-band excitation can be misleading. Consequently, sinusoidal signals are predominantly used here in numerical simulations and for experimental verification. However, the approach is equally applicable to non-sinusoidal waveforms, as its use in active vibration control [6] demonstrates.

In the experiments, the estimates from the three-sensor, near-field array were compared with estimates from a two-sensor array mounted on the beam but located in the far field. Since the damping in the beam is very small, the propagating waves at the two sensor array locations have the same amplitudes but different phases. However, because the wave motion is dispersive, different frequency components take different times to travel between the arrays and hence direct comparison in the time domain is not meaningful except for time harmonic behaviour.

The outputs from these two sensors were filtered using the results of Ref. [2], which assume that far-field conditions exist. The accuracy of these measurements is relatively well established. The outputs of the three sensors were filtered using the near-field filters described above. Various experimental configurations were investigated and two are shown in Fig. 13. The first is intended to investigate the far-field performance and to verify that estimates from the near-field array are the same as those provided by the more established far-field technique. The second configuration is one in which there are known relations between the wave amplitudes.

The first series of experiments involved discrete frequency excitation with all three accelerometers (A_1, A_2 and A_3) located in the far field as shown in Fig. 13(a). The signals from the outer sensors A_1 and A_3 were filtered using the far-field method of Ref. [2]. This allows the performance in the far field to be assessed. Fig. 14 shows an example. The estimates of the amplitudes of the propagating wave components using both the near-field and far-field arrays

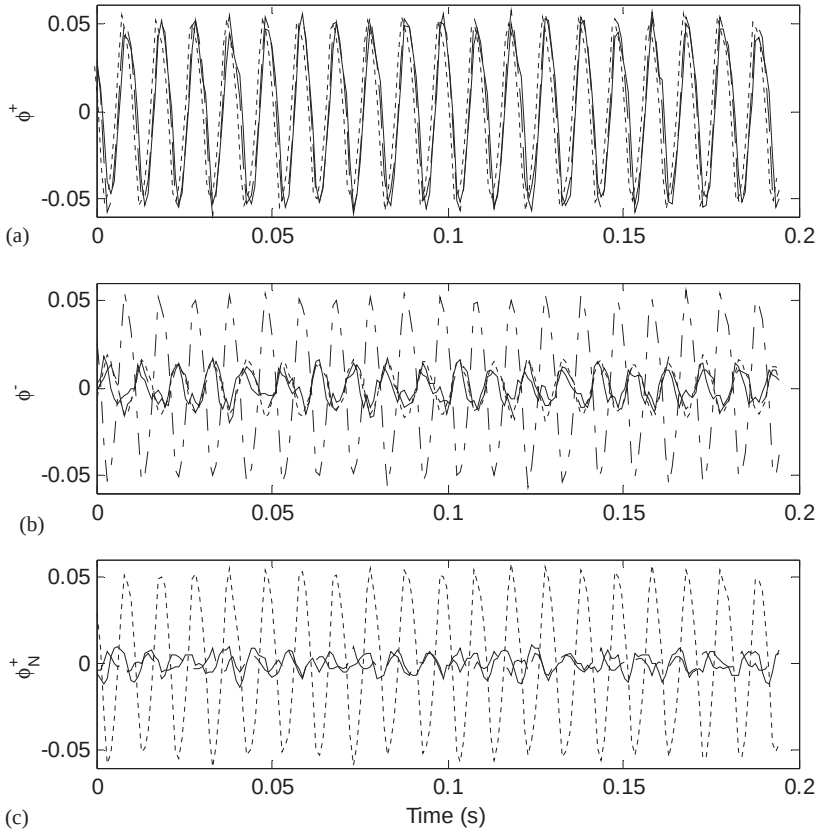

Fig. 14. Estimated amplitudes of wave components using near-field array, sinusoidal disturbance at 100 Hz: configuration 1, array located in the far field; (· · · ·) estimates from far-field array, $n_d = 15$: (a) —— $\phi^+(t)$, $n_d = 5$, ----- $\phi^+(t)$, $n_d = 15$; (b) —— $\phi^-(t)$, $n_d = 5$, ----- $\phi^-(t)$, $n_d = 15$; -.--. $\phi^+(t)$ far-field array; (c) —— $\phi_N^+(t)$, $n_d = 5$, -.--.-.- $\phi_N^+(t)$, $n_d = 15$; · · · · $\phi^+(t)$ far-field array.

agree well. There is little difference between the estimates provided by the near-field array with $n_d = 5$ or 15. The estimated amplitudes of the near-field wave are much smaller than those of the propagating waves. It should of course be almost zero, but a non-zero estimate is produced due to cross-sensitivity, noise, filter inaccuracy, etc.

In the second series of experiments, the sensors were mounted as shown in Fig. 13(b). Broadband excitation in the 51–460 Hz frequency band was applied. The three-sensor array is mounted in the near field at the end of the beam, while the two-sensor array is once again in the far field. This arrangement enables the broadband performance to be assessed when a near field exists. In Fig. 15(a), the spectral densities of the estimated amplitudes of the propagating waves are compared. The spectral densities of the amplitudes of both positive and negative going wave components, estimated using both the near- and far-field arrays, are nearly equal, as one would expect since there is little energy dissipation in this region of the beam. The disagreement at low frequencies (and, to a lesser extent, at high frequencies) arises from the different forms taken by the near-field and far-field filters and the weighting that has been applied to the estimation of the filter coefficients.

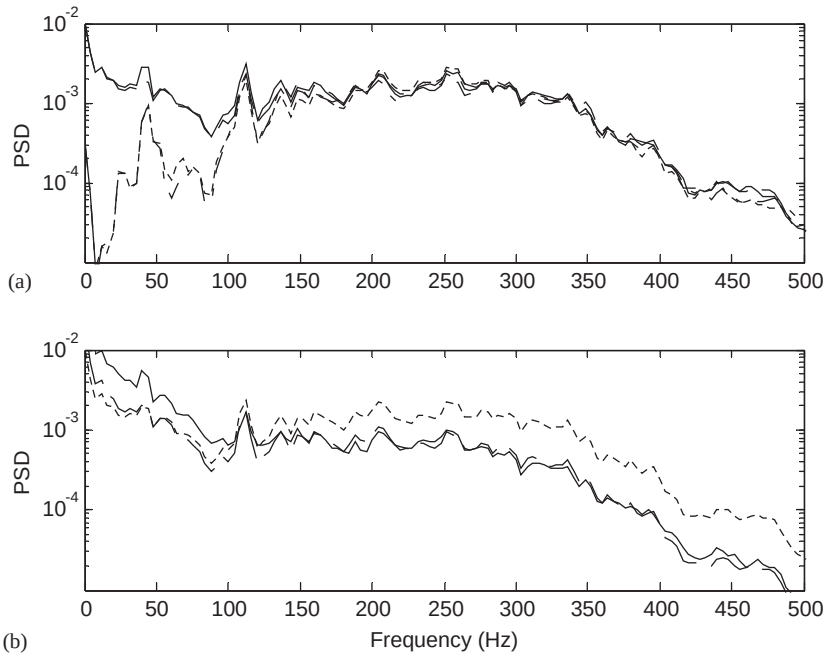

Fig. 15. Spectral densities of the estimated amplitudes of the wave components, $n_d = 5$: (a) —— ϕ^+, near-field array; ----- ϕ^-, near-field array; $\cdots\phi^-$, far-field array; -.-.-.- ϕ^+, far-field array; (b) ----- ϕ^-, near-field array; —— ϕ_N^+, near-field array; –––– ϕ_N^+, theoretical.

The estimate of the amplitude of the near-field wave component is shown in Fig. 15(b). The positive-going propagating wave should have the same magnitude as the negative-going propagating wave, since the magnitude of the reflection coefficient is 1, and this behaviour is observed. However, the magnitude of the near-field wave component should be $\sqrt{2}\exp(-kd)$ times that of the negative going wave, where $d = 0.066$ m. This is because the reflection coefficient at the free end is $(1 - i)$ and the near field attenuates over a distance of 0.066 m from the free end to the centre of the sensor array. This theoretical estimate is also shown in Fig. 15(b) and agrees well with the measured amplitude.

6. Concluding remarks

This paper concerned how filters can be designed to provide real-time estimates of the amplitudes of the various flexural wave components in a beam vibrating in bending. It was assumed that two propagating components and a single near-field wave are present. The outputs of three sensors are filtered, with the filters being designed in the frequency domain and implemented in the time domain as FIR filters. Performance issues were considered, numerical examples presented and an experimental implementation described. Application to the measurement of structural intensity was briefly described, with application to active vibration control being considered in some detail elsewhere [6]. The method can be extended

straightforwardly for arrays comprising sensors of different types (e.g. some combination of strain gauges, piezoelectric patches and accelerometers), or an over-determined array comprising four or more sensors could be used to improve accuracy—the only substantive difference is in the form of the sensor matrix $\mathbf{S}$ of Eq. (7). The same approach can also be used if both positive-going and negative-going near fields are considered, except that at least four sensors are required (see Appendix A).

Generally, filters of only moderate order provide accurate, robust estimates except at low and high frequencies. There is a trade-off in the length of the FIR filters between accuracy (large n_d) and small group delays (small n_d), and hence the best choice of filter length would depend on the specific application in mind—for active control processing delays are probably more important, while for intensity measurement accuracy is likely to be more important.

Acknowledgements

The first two authors gratefully acknowledge the financial assistance provided by the New Zealand Foundation for Research, Science and Technology.

Appendix A. Two near-field waves

If both near fields are significant, the wave components can be measured using an array of at least four sensors. The approach is the same as that described in Section 2 except that the sensor matrix $\mathbf{S}(\omega)$ is different and hence so, too, are the frequency and impulse response matrices $\mathbf{G}(\omega)$ and $\mathbf{g}(t)$.

Consider the case of four displacement sensors attached at the four points (x_1, x_2, x_3, x_4). The displacement of the beam at frequency ω is given by Eq. (3) as the sum of wave components. Hence the vector of sensor outputs is

$$\mathbf{Y}(\omega) = \begin{Bmatrix} W(x_1,\omega) \\ W(x_2,\omega) \\ W(x_3,\omega) \\ W(x_4,\omega) \end{Bmatrix} \tag{A.1}$$

and hence

$$\mathbf{Y}(\omega) = \mathbf{S}(\omega)\mathbf{\Phi}(\omega), \quad \mathbf{\Phi}(\omega) = \begin{Bmatrix} \Phi^+ \\ \Phi^- \\ \Phi_N^+ \\ \Phi_N^- \end{Bmatrix}, \tag{A.2}$$

where the sensor matrix

$$\mathbf{S}(\omega) = \begin{bmatrix} e^{-ikx_1} & e^{ikx_1} & e^{-kx_1} & e^{kx_1} \\ e^{-ikx_2} & e^{ikx_2} & e^{-kx_2} & e^{kx_2} \\ e^{-ikx_3} & e^{ikx_3} & e^{-kx_3} & e^{kx_3} \\ e^{-ikx_4} & e^{ikx_4} & e^{-kx_4} & e^{kx_4} \end{bmatrix}. \tag{A.3}$$

The vector of wave amplitudes $\mathbf{\Phi}(\omega)$ is again given by Eq. (8). Since $\mathbf{S}$ is (at least) 4×4 the situation is best treated numerically, by inverting $\mathbf{S}$ to find $\mathbf{G}(\omega)$.

References

[1] G. Pavic, Measurement of structure borne wave intensity, Part 1: formulation of the methods, *Journal of Sound and Vibration* 49 (1976) 221–230.

[2] B.R. Mace, C.R. Halkyard, Time domain estimation of response and intensity using wave decomposition and reconstruction, *Journal of Sound and Vibration* 230 (3) (2000) 561–589.

[3] C.R. Fuller, S.J. Elliott, P.A. Nelson, *Active Control of Vibration*, Academic Press, San Diego, 1996.

[4] C.R. Halkyard, B.R. Mace, Feedforward adaptive control of flexural vibration using wave amplitudes, *Journal of Sound and Vibration* 254 (1) (2002) 117–141.

[5] C.R. Halkyard, B.R. Mace, Adaptive control of flexural vibration in the presence of a nearfield, *Proceedings of Internoise*, The Hague, The Netherlands, 2001.

[6] C.R. Halkyard, B.R. Mace, Adaptive active control of flexural waves in a beam in the presence of a nearfield, *Journal of Sound and Vibration* 285 (1 + 2) (2005) 149–171.